Proceedings of the Second International Workshop on
Fundamental Issues and Future Research Directions for Parallel Mechanisms and Manipulators
September 21–22, 2008, Montpellier, France
N. Andreff, O. Company, M. Gouttefarde, S. Krut and F. Pierrot, editors

A fluidic-muscle driven force-controlled parallel platform for physical simulation of virtual spatial force-displacement laws

ANDRÉS KECSKEMÉTHY
Lehrstuhl für Mechanik und Robotik
Universität Duisburg-Essen
D-47057 Duisburg

KUSNADI LIEM
Lehrstuhl für Mechanik und Robotik
Universität Duisburg-Essen
D-47057 Duisburg

MAHENDRA DHANU SINGH
Lehrstuhl für Mechanik und Robotik
Universität Duisburg-Essen
D-47057 Duisburg

Abstract:
Described in this paper is a novel six-legged parallel platform driven by fluidic muscles. The advantage of the platform is that it is virtually free of stick-slip effects. Thus, the device is well-suited for fine-tuned force control and for physical simulation of virtual force-displacement laws. The legs of the platform are of type RRPS and are equipped with a coaxial coil spring and a fluidic muscle providing push and pull forces. Each leg is equipped with a force sensor, a pressure sensor and a magnetostrictive position encoder. The control scheme for the platform comprises six control loops for the six operated actuators with model-based force control comprising individual gas models as well as the rubber nonlinearities for each leg. The control law also includes the gas flow in the proportional directional control valve in 3/3-way function. The present paper describes the basic architecture of the platform, the dynamic models as well as testbed results for the existing fluidic-muscle parallel platform DynaHex. It is shown that the presented control scheme leads to a stable force control of the platform for quasi-static motion. As an application, the device will be employed in fields of biomechanics, as well as in general environments requiring physical simulation.

1 Introduction

Parallel platforms are well-established today and are available in multiple architectures and technologies [6]. In this setting, most parallel platforms are position controlled [1]. A special kind of task results when the parallel manipulator is targeted to provide force control. In these cases, one seeks to control the actuators such that a given force at the end-effector is achieved. Current methodologies are based on hybrid force/position control schemes, where the actuators are velocity-controlled with some assumptions on the compliance of the environment [18]. For example, the force-impedance control scheme proposed in [12] implemented uses a robot system that consists of an industrial serial six-axis robot and a small six DOF parallel manipulator fixed at its flange. By this approach, the merits of the large workspace of the serial robot are combined with the high bandwidth of the parallel platform driven by electric motors. This concept is also used e.g. for industrial force-feedback control [14]. However, in some applications, such as very stiff environments, or in environments with unknown or discontinuous stiffness properties, direct force control would be more desirable. An example of such an application is a testing device for cervical pairs [11], where facet joint contact unsteadily occurs and would be destroyed by errors in position control. An approach to circumvent this problem is the use of fluidic muscles, which have the advantage of avoidance of slip-stick effects, and also have a very good transmission behaviour between pressure and force. Additional advantages of fluidic muscles are their small size with respect to achievable forces, as well as their long durability. Pneumatic muscles are already used to control the pose of parallel platforms [19]. By active force control, such fluidic muscles can produce any desired force-displacement law. In this paper, we analyse the use of pneumatic muscles for directly controlling the force at the platform. Although they are more difficult to control, we make use of the compliance and direct force controllability to improve the end-effector behaviour when sudden contact arises.

The optimal design of the platform has to take into account the problems of singularity avoidance [13], optimization of manipulability index [17] and dexterity index [15], direct kinematics computation [4], as well as general technological issues [6]. A solution to these problems can be found by interval analysis with the software package ALIAS [7], used in the present work.

This design task is described in the first part of the present paper, the modeling and control of the pneumatic muscles are described in the second part and finally, experimental results obtained with the developed force controller are presented.

2 Basic Design of the Platform

2.1 Basic structure

For the realization of the targeted platform, a six-legged $RR\underline{P}S$-type parallel platform [6] was chosen, each leg being hinged by a universal joint (RR) at the base and a spherical joint (S) at the platform, with a prismatic joint along its leg axis as input stroke (Fig. 1).

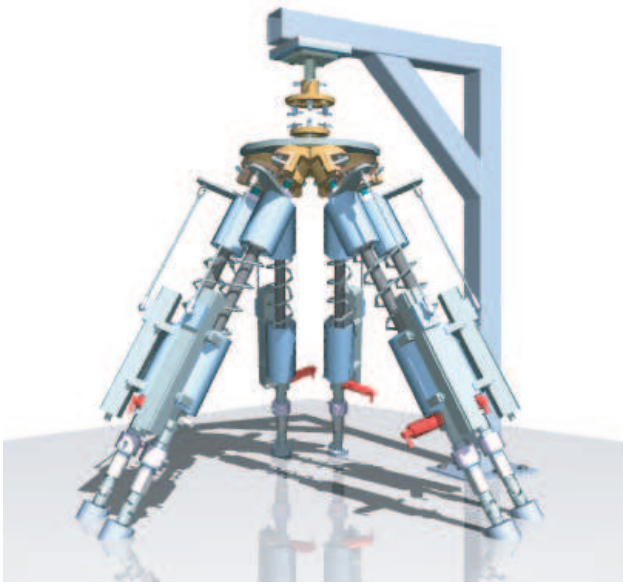

Figure 1: Developed parallel manipulator

In order to avoid slip-stick effects, the actuators are chosen as fluidic (pneumatic) muscles (MAS 20, Festo AG & Co. KG., [9]), which operate by contracting in axial direction when inflated.

2.2 Actuators

As a fluidic muscle can only produce pulling forces, an additional force element is required in order to provide also a push force. This is realized in the present context by embedding the fluidic muscle into a coaxial coil spring whose stiffness is determined such that the required maximal pushing forces can be obtained within the stroke of the fluidic muscle (Fig. 2). Each actuator is equipped with sensors measuring force, pressure and stroke, as illustrated in Fig. 2. The stroke of the hybrid actuator depends on the specific type of the fluidic muscle and its length. For the chosen fluidic muscle the stroke is $\Delta\rho = 40$ mm.

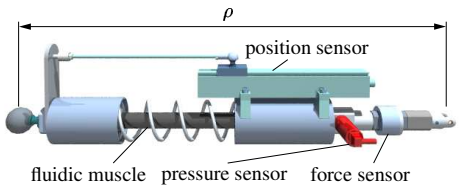

Figure 2: Force, position and pressure sensor

The relationship between air pressure and contraction force is nonlinear and depends on the actual length of the muscles (Fig. 3).

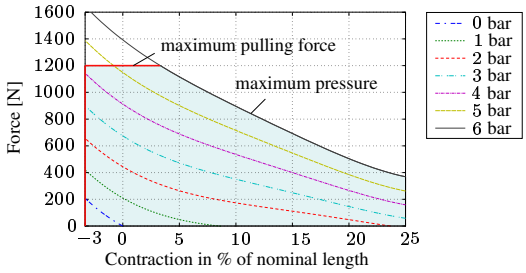

Figure 3: Force-contraction curves of fluidic muscle

The maximal and minimal actuator forces F_{min}, F_{max} depend on the current length ρ of the actuator due to the nonlinear characteristic of the fluidic muscle: at a constant pressure the muscle force decreases if the contraction increases. The corresponding maximal and minimal forces in [N] at the attachment point of the platform ("+" = pull, "-" = push) are plotted for the current actuators in Fig. 4. The corresponding relationships can also be approximated by the equations

$$F_{min} = 7\ \frac{\mathrm{N}}{\mathrm{mm}}\ \rho - 4,768.5\ \mathrm{N}$$

$$F_{max} = 0.304\ \frac{\mathrm{N}}{\mathrm{mm}^2}\ \rho^2 - 361.3\ \frac{\mathrm{N}}{\mathrm{mm}}\ \rho + 107,095.7\ \mathrm{N}$$

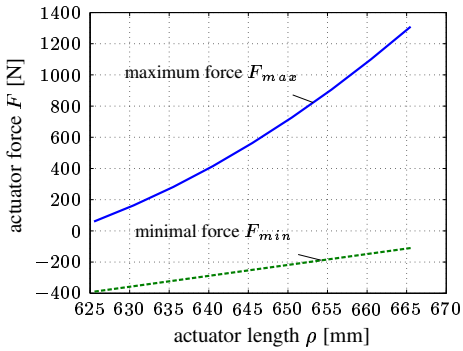

Figure 4: Maximal and minimal actuator forces as function of actuator length

2.3 Platform parameters

As basic design concept for the platform, a *symmetric simplified manipulator* [5] was chosen, where the attachment points at the base and the platform are located along the edge of a circular

disk in three symmetrically distributed pairs of attachment points, respectively (Fig. 5). Thus as design parameters one only has the relative angle offsets α_A and α_B and the circle radii r_a and r_b at base and platform, respectively. This design has many advantages in manufacturing.

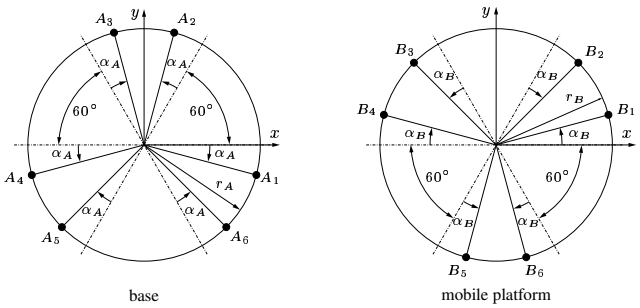

Figure 5: Attachment points of the joint center

As an additional design parameter, the height h_{EE} of the end-effector location with respect to the plane passing through the platform spherical joints (Fig. 6A) was considered. As will be seen, this parameter has significant influence on the required stroke of the actuators for completing a given platform motion.

A further important issue was the manufacturing of the spherical joints, which needed to feature significant tilt angles in order to allow for the desired large roll and pitch angles of the platform. For this purpose, a customized version was built consisting of a two-piece socket manufactured in a combination of milling and turning. With the chosen spherical joints, a tilt angle of 25° was made possible (Fig. 6B).

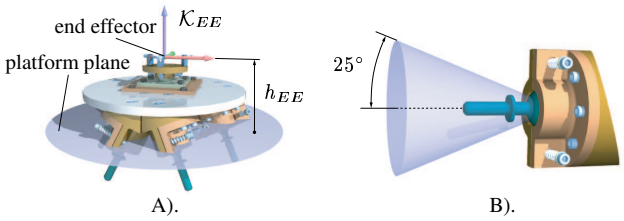

Figure 6: A) Distance of the end effector from the platform plane. B) Limit of spherical joint

For the placement of the hinge points at base and platform, a theoretical investigation of the best placement points was conducted in [11] which is briefly reproduced here for better understanding of the underlying concept.

The design consisted of the phases: (1) finding a singularity-free basic configuration, and (2) verifying by interval analysis that the platform will achieve the expected results (stiffness, collision-avoidance, limited stroke, expected forces) within the targeted workspace.

In order to achieve a singularity-free design of the platform, the determinant of the inverse of the end-effector Jacobian $\mathbf{J}_{EE}^{-1}$ should be far from zero, which corresponds to a large "manipulability index" [17]. Here, the authors gratefully acknowledge the kind support of Prof. Manfred Husty from the University of Innsbruck in applying analytical methods for avoiding such singularities in the complete workspace. The end-effector Jacobian $\mathbf{J}_{EE}$ hereby maps infinitesimal length changes $\delta\boldsymbol{\rho}$ of the legs to corresponding infinitesimal variations $\delta\underline{\mathrm{t}}_{EE}$ of the platform pose at the end effector:

$$\delta\underline{\mathrm{t}}_{EE} = \mathbf{J}_{EE}\,\delta\boldsymbol{\rho} \ . \tag{1}$$

For the given architecture, it is easier to compute the inverse $\mathbf{J}_{EE}^{-1}$ of the Jacobian than the Jacobian itself, which could be done using kinematical differentials [8]. This method is referred to as velocity-based determination of Jacobians (*column-wise evaluation*) and is not reproduced here in order to save space, as the corresponding equations are trivial to the parallel platform community.

A possible, plausible criterion for the design of the platform is minimizing the required stroke to move the platform, such as to have large platform motions with restricted fluidic muscle strokes. To this end, first, the stroke as a function of angle α_A was regarded, showing that the minimal stroke is attained for $\alpha_A = \alpha_B$, and in particular for $\alpha_A = 0°$. However, the manipulability index at this point always have a minimum equal to zero, meaning that a configuration $\alpha_A = \alpha_B$ is singular. Hence, this optimizing criterion is not suitable for the platform design.

As a second possibility, the dependency of the leg stroke on the end-effector offset was regarded. This is shown in Fig. 7, where the stroke is plotted over the upper platform radius for different values of the platform offset. As can be seen, an operation point below of the platform always leads to higher required stroke, while positive offset values reduce the amount of the required stroke. Taking $h_{EE} = 125\,\mathrm{mm}$, one can obtain a stroke of 40 mm at the prescribed upper radius of 100 mm, which is a realistic stroke for the chosen fluidic muscles. At this value, the manipulability index at the home position renders a value of 5.9 E+5 m^{-3} , which is acceptable. This shows that choosing a suitable operation point is crucial for a good behavior of the platform.

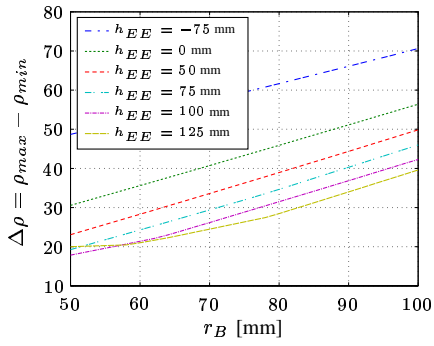

Figure 7: Stroke as function of h_{EE} and r_B ($\alpha_A = -20°, \alpha_B = 5°$)

In addition to singularity, the range of motion and the target forces of the end-effector were analyzed using the interval-arithmetic library ALIAS [7]. Hereby, the functional verification of the platform is carried out using the maximal stroke values, which were set to $\rho_{min} = 625.5\,\mathrm{mm}$ and $\rho_{max} = 665.5\,\mathrm{mm}$.

3 Modeling and control of fluidic muscle

3.1 Model of the fluidic muscles

For developing a model-based control, the characteristics of each fluidic muscle were identified by individual measurements due to possible differences in the six actuators. At first the relationship between force F on the one side, and stroke s and pressure p on the other (as depicted by Fig. 4) was approximated by a ninth order polynomial:

$$F = g(s,p) \approx \sum_{i,j=0}^{i+j\leq 9} a_{ij} s^i p^j \tag{2}$$

The coefficients were obtained from experiments and data fitting using least squares [2].

For the dynamic gas model, we regard the ideal gas law and the polytropic equation

$$pV = mRT \ , \tag{3}$$
$$p\rho^{-\gamma} = \text{const.} \ , \tag{4}$$

from which after taking the time derivative one obtains

$$\dot{p} = \gamma \frac{RT}{V}\dot{m} - \gamma \frac{p}{V}\dot{V} \ , \tag{5}$$

where ρ, R, T, V and m denote the density, gas constant, temperature, volume of the fluidic muscle and gas mass, respectively.

For the performed actuations it can be assumed that the volume of the fluidic muscle only depends on the stroke. We approximate this volume-stroke dependency displayed in Fig. 8 by

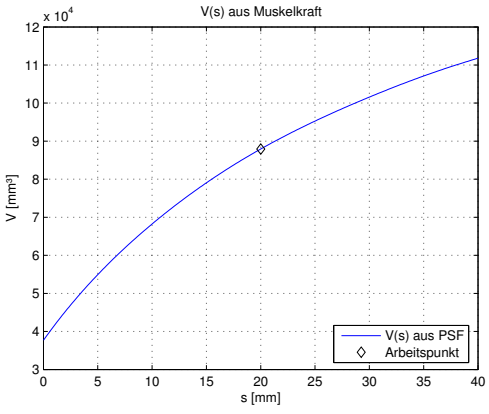

Figure 8: Volume of pneumatic muscle over stroke

a third order polynomial

$$V(s) = \sum_{i=0}^{3} b_i s^i \tag{6}$$

leading to the time derivative

$$\dot{V} = \frac{\mathrm{d}V(s)}{\mathrm{d}t} = \frac{\mathrm{d}V(s)}{\mathrm{d}s}\dot{s} = \left(\sum_{i=1}^{3} i b_i s^{i-1}\right)\dot{s}. \tag{7}$$

The mass flow $\dot{m}$ with which the muscle is inflated has a nonlinear characteristic and is a function of pressure p inside the muscle and the input voltage u of the valve

$$\dot{m} = \phi(p,u) \ , \tag{8}$$

where the supply pressure is assumed to be constant and the function $\phi(p,u)$ is still unknown.

By substituting (8) and (7) into (5), one obtains the representation for $\dot{p}$

$$\dot{p} = \underbrace{\gamma \frac{RT}{V(s)}\phi(p,u)}_{f_1(s,p,u)} - \underbrace{\gamma \frac{p}{V(s)}\frac{\mathrm{d}V(s)}{\mathrm{d}s}\dot{s}}_{f_2(s,p,\dot{s})} \ . \tag{9}$$

which can be viewed as a superposition of two terms

$$\dot{p} = f_1(s,p,u) + f_2(s,p,\dot{s}) \tag{10}$$

In Eq. (10), the second term can be readily computed once the approximation $V(s)$ is known (from measurements) and the pressure is given.

The difficult term in Eq. (10) is the first term, as the nonlinear valve function $\phi(p,u)$ is problematic to measure. In the sequel, we propose an alternative way of determining this term, based on an interpretation that makes its measurement easier.

Assume the position of the actuator to be constant. Then, for the velocity it holds $\dot{s} = 0$, and the second term of the right side of the equation vanishes. Thus the first term in (10) is just the pressure rate for fixed actuator length and given voltage and pressure values

$$\hat{\dot{p}}_s(p,u) = \dot{p}(s,p,u)\Big|_{s=\text{const.}} \ . \tag{11}$$

In order to determine this two-parametric function, the actuator is fixed into a rigid frame at different lengths and then voltage step functions of the amplitude u are applied to the fluidic muscle starting at $p = 0$. From the resulting transient pressure step response and the ensuing time histories, the slopes at different times and thus also at different pressures can be determined numerically, yielding a field of slopes for each voltage step response (Fig. 3.1).

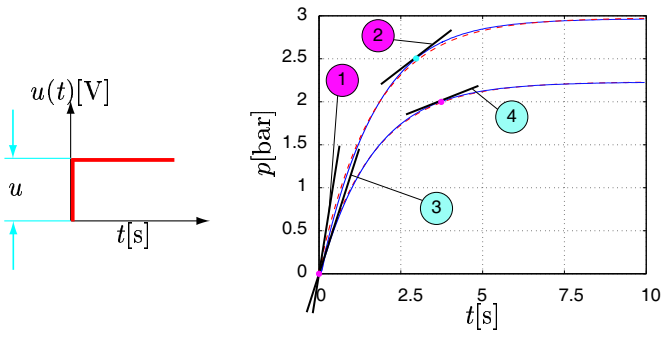

Figure 9: Pressure responses of voltage step signals for generation of $\hat{\dot{p}}$-surface

By distributing the computed slopes at the corresponding parameter pairs $u, p(t)$, one obtains a parametric representation of the surface $\hat{\dot{p}}_s$ for each given fluidic muscle length (Fig. 3.1). These parametric surfaces can be repeated for several fluidic muscle lengths and can then be used to compute the first term in (9) for any value of p, u and s.

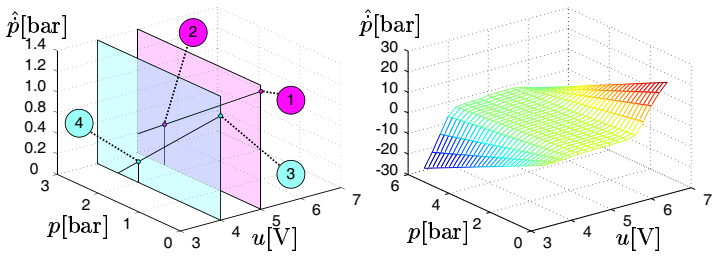

Figure 10: Generation of $\hat{\dot{p}}(p, u)$ surface for fixed s

It should be noted that the procedure must be repeated for pressure decreases resulting from a closing valve, as the corresponding coefficients and thus the parametric surfaces for pressure decrease are different than those for pressure increase.

This method of collecting the pressure rates resulting from the voltage step functions into a parametric surface now be improved by the following semi-analytic approach. From the step response time histories in Fig. 3.1, one can recognize that these are quite close to exponential functions. By parameterizing these exponential functions for fixed stroke s (see [3]) as

$$\hat{\dot{p}}^{\text{appr}}_{\text{inc}}(t;u)|_{u=\text{const.}} = k_1(u)(1 - e^{-k_2(u)t}) + k_3(u) \qquad (12)$$

one can determine the coefficients $k_1(u), k_2(u)$ and $k_3(u)$ from least squares fitting of the parametrized exponential function with the measured step responses for constant actuator strokes s and constant valve voltage step functions u. The time derivative of the exponential approach then leads to following expression:

$$\hat{\dot{p}}^{\text{appr}}_{\text{inc}}(u) \quad = \quad k_1(u)k_2(u)e^{-k_2(u)t} \qquad (13)$$

After resolving Eq. (12) for the exponential function and back-substituting this expression into Eq. (13), one obtains the approximation of the pressure rate (for fixed u and s) as

$$\hat{\dot{p}}^{\text{appr}}_{\text{inc}}(u) \quad = \quad k_2(u) \cdot (k_1(u) + k_3(u) - p) \qquad (14)$$

which shows that the pressure rate is approximately a linear function of the pressure.

For pressure decreases a corresponding exponential function

$$p^{\text{appr}}_{\text{dec}}(t;u) = k_1(u)e^{-k_2(u)\,t} + k_3(u). \qquad (15)$$

is used as approximation, where the parameters $k_1(u), k_2(u), k_3(u)$ are again determined from the corresponding measurements and least squares fitting. For the time derivative one then obtains:

$$\hat{\dot{p}}^{\text{appr}}_{\text{dec}}(u) \quad = \quad -k_1(u)k_2(u)e^{-k_2(u)t} \qquad (16)$$

which after re-substituting the corresponding expression for the exponential function analogously to Eq. (14) leads to

$$\hat{\dot{p}}^{\text{appr}}_{\text{dec}}(u) \quad = \quad k_2(u) \cdot (k_3(u) - p) \qquad (17)$$

which again is a linear expression in p..

Using the experimentally established function $f_1(s, p, u)$, the nonlinear valve characteristic $\phi(p, u)$ can be determined easily. This was achieved by inflating and deflating a closed pressure vessel, yielding the parameter surface displayed in Fig. 11. Dynamical effects of the magnetic slide inside the valves are neglected.

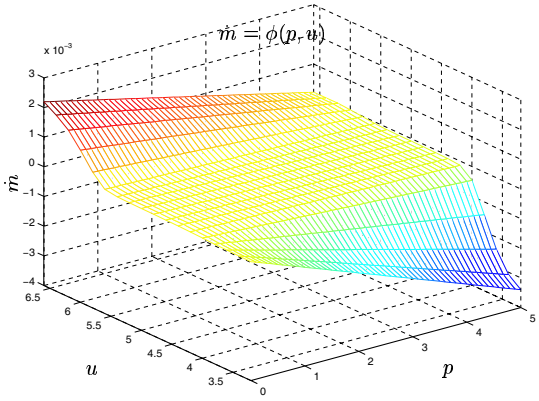

Figure 11: Experimentally measured mass flow

3.2 Force control

The task of force control is to determine a target voltage U^T which will achieve a given target force F^T at the actuator.

To determine this relationship, one has on the one hand the force relationship from Eq. (2), which can also be parametrized (for fixed s) as a univariate function of pressure p

$$F = g(s, p) = g_s(p) \qquad (18)$$

On the other hand, one has the differential equation Eq. (10), which, after resolving for the first term, yields

$$\hat{f}_{1(s,p)}(u) = f_1(s, p, u) = \dot{p} - f_2(s, p, \dot{s}) \qquad (19)$$

For given stroke s, stroke rate $\dot{s}$ and pressure p, Eq. (19) can be regarded as a univariate function $\hat{f}_{1(s,p)}(u)$ of u which can be resolved for the target voltage as

$$u(p, s, \dot{s}) = \hat{f}^{-1}_{1(s,p)} \{\dot{p} - f_2(s, p, \dot{s})\} \quad . \qquad (20)$$

In order to evaluate this equation, one needs approximations for the stroke rate, the target pressure and the target pressure rate at any state of the system. These are proposed to be determined as follows.

The stroke rate can be approximated by backward finite differences

$$\hat{\dot{s}}(t_i) = \frac{s(t_i) - s(t_{i-1})}{t_i - t_{i-1}}; \quad \hat{\dot{s}}(t_0) = 0 \qquad (21)$$

The target pressure p^T is obtained from the inverse of the univariate force-pressure function of Eq. (2) as

$$p^T = g_s^{-1}(F^T) \tag{22}$$

Finally the target pressure rate is approximated by a virtual pressure rate $\tilde{\dot{p}}^T$ obtained by the assumption that the target pressure p^T will be achieved from the current pressure p after some time delay ΔT. The interpretation of this approach then yields

$$\tilde{\dot{p}}^T(t_i) = \frac{p^T(t_i) - p(t_i)}{\Delta T} \tag{23}$$

Thus, one obtains the target voltage as

$$U^T(t) = \hat{f}_{1,s,p}^{-1}\left(\tilde{\dot{p}}^T + p\frac{\mathrm{d}V(s)}{\mathrm{d}s}\hat{\dot{s}}\right) \tag{24}$$

By putting all equations together the block diagram given in Fig. 12 is obtained. Here the target force and the measured position are inserted into the first inverse model yielding the target pressure, which then is subtracted from the measured pressure and divided by ΔT, yielding the virtual pressure rate. The measured position, the approximated velocity, the measured pressure and the virtual pressure rate are inserted into the second inverse model yielding the target voltage. In case of perfect inverse models, the measured force is equal to the target force, but however due to model inaccuracies, there is a remaining error which is inserted into a PID controller generating a correcting voltage which then is added to the target voltage. The total voltage U then is sent to the valve which inflates or deflates the actuator. This actuator control was implemented on the real time system dSPACE.

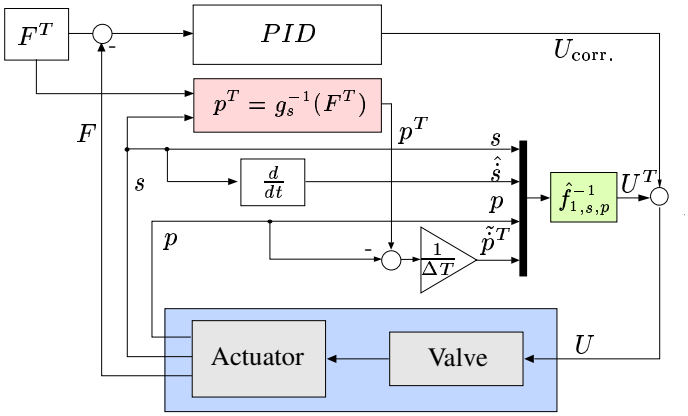

Figure 12: Actuator control scheme

3.3 Flatness based control

An alternative for force control is a flatness-based approach, for which however the trajectory must be known. The character of a flat system is that (1) it has the same number of inputs and outputs, (2) the system inputs and the system states can be computed by using the system outputs and their derivatives [16]. For a position control, the position s of the fludic muscle can be chosen as system output and the mass flow rate $\dot{m}$ through the valve can be chosen as the system input. Thus the first condition for a flat system is fulfilled. With Eq. (8) and Eq. (9) the plant takes the state-space form

$$\dot{\boldsymbol{x}} = A(\boldsymbol{x}) + B(\boldsymbol{x})u_{in} \tag{25}$$

$$y = C(\boldsymbol{x}) \tag{26}$$

where [10]:

$$\begin{bmatrix} \dot{p} \\ \dot{s} \\ \ddot{s} \end{bmatrix} = \begin{bmatrix} -\frac{\gamma}{V}\dot{V} \\ \dot{s} \\ \frac{F_A - m_b g - F_R}{m_b} \end{bmatrix} + \begin{bmatrix} \frac{\gamma}{V}RT \\ 0 \\ 0 \end{bmatrix} u_{in} \tag{27}$$

$$y = s\,, \tag{28}$$

and $u_{in} = \dot{m}$. Here, F_A is the fluidic muscle force, m_b is the platform mass, and F_R is the spring force. Using Eq. (2), the state space vector $\boldsymbol{x} = [\,p,\ s,\ \dot{s}\,]^{\mathrm{T}}$ can be expressed by $s, \dot{s}$ and $\ddot{s}$:

$$\boldsymbol{x} = \begin{bmatrix} \sum_{i,j=0}^{i+j\leq 7} a_{ij}(m_b\ddot{s} + m_b g + F_R)^i s^j \\ s \\ \dot{s} \end{bmatrix} \tag{29}$$

By differentiating the acceleration $\ddot{s}$ with respect to time and resolving the equation for $\dot{p}$ one obtains

$$\dot{p} = \frac{m_b\dddot{s} + \frac{\mathrm{d}F_R}{\mathrm{d}t} - \dot{s}\sum_{i,j=0}^{i+j\leq 6} i a_{ij} s^{i-1} p^j}{\sum_{i,j=0}^{i+j\leq 6} j a_{ij} s^i p^{j-1}}\,. \tag{30}$$

Thus, the input $\dot{m}$ can be calculated from Eq. (5) as

$$\dot{m} = \frac{1}{RT}\left(\frac{V(s)}{\gamma}\dot{p} + \frac{\mathrm{d}V(s)}{\mathrm{d}s}\dot{s}p\right)\,, \tag{31}$$

where Eq. (30) is used to compute $\dot{p}$.

4 Results

4.1 Manufactured platform

The above-derived procedure was implemented on a realization of the platform, as shown in Fig. 13. The hexapod is controlled by a DS 1005 system from dSPACE. The platform can lift approximately 100kg when all actuators are activated to their maximal push/pull values. For the force control runs described below, the platform was fixed by a rigid shaft which was fixed to a raft, such as to be able to hold the strokes of the actuators fixed.

4.2 Actuator force control

Each actuator was individually measured, and it turned out that the parametric surfaces for the actuators could diverge substantially, although the same standard components were employed. Thus, the platform model requires individual validation for each component in order to yield acceptable results First steps using a linear PID control without inverse model showed an unstable behavior due to this nonlinear relationship between pressure/force and stroke. Measurements showed that the relationship between force and pressure was almost proportional with a very high gain from pressure to force. One could verify that a variation of 10 mbar leads to an oscillation of 3 N. This means that

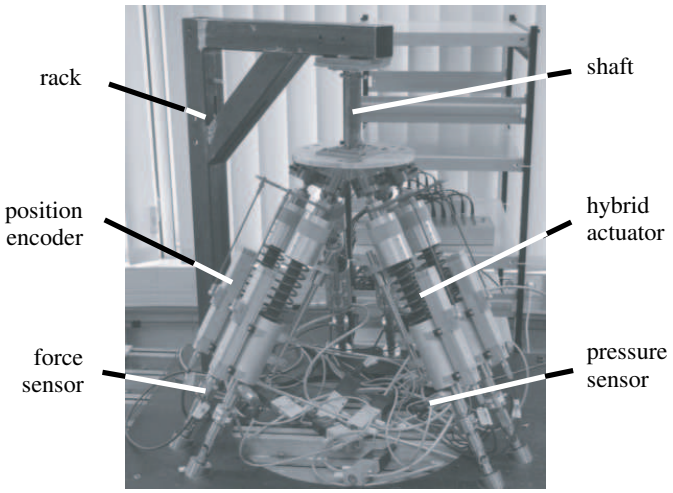

Figure 13: Hexapod

due to the accuracy of the pressure sensors only a force control with an accuracy of 3 to 4 N is feasible. Fig. 14 shows the result of the model-based force control for a prescribed sinusoidal target force. Due to the instability resulting from rapid changes of the target force, a period of 80 sec needed to be chosen. Thus the control is currently suitable only for quasi-static changes. The amplitudes are +/- 200 N and it can be seen that the error between target and measured force is below 3 N. Due to the amplifications of the pressure variations explained above, the error value can not be further reduced.

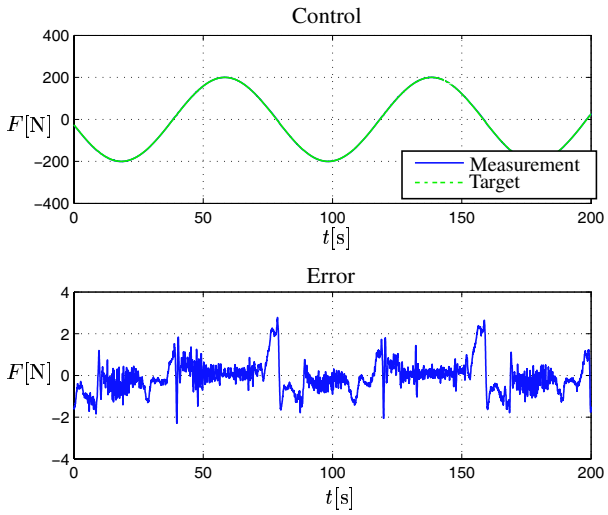

Figure 14: Result of single actuator force control

4.3 Force control of the complete platform

The model-based force control of the single actuator was embedded into the force control of the platform. The aim was to transmit the target forces/torques given by the computer simulation to the end effector of the platform. The first task is to determine the six target actuator forces $Q_i, i = 1, \ldots, 6$ for a given wrench $\underline{\mathrm{w}}_{EE}$ at the end-effector $\mathcal{K}_{EE}$ (Fig. 15). Hereby, a wrench consists of a moment and a force applied to the origin of the reference frame. The corresponding transmission equation for an ideal platform (neglecting friction) is known to be

$$\underline{Q} = \mathbf{J}_{EE}^{T}\, \underline{\mathrm{w}}_{EE} \quad . \tag{32}$$

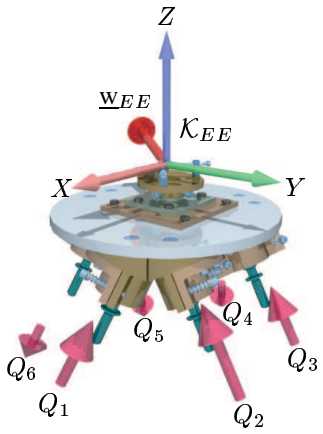

Figure 15: Forces at platform

For the actual control, the platform target wrench $\underline{\mathrm{w}}_{EE}$ is mapped to the actuator forces using a more elaborate model programmed with the multibody C++ library Mobile [8] using the kinetostatic transmission method and simple friction models.

The target forces are then transmitted to the dSPACE control unit using the interface CLIB (Fig. 16). The control unit itself computes the 6 model based control loops yielding the voltage signals at the six actuators of the hexapod. The feedback is given by 18 sensors measuring the pressure, force and position of each actuator. Again, after implementing the force control one could verify that only quasi-static changes in force could be tracked, while faster force changes lead to instability.

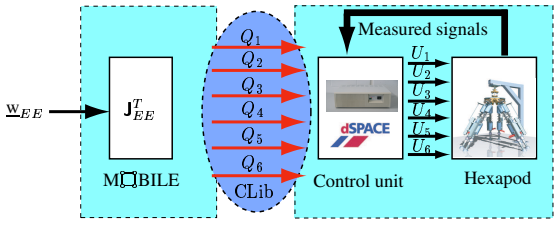

Figure 16: Platform control scheme

Fig. 17 shows a test run with pure target force prescription (no moment) at the platform. The force prescription is divided into three steps, with a pure x load $\boldsymbol{F_{EE}} = \begin{bmatrix} -40\mathrm{N} & 0\mathrm{N} & 0\mathrm{N} \end{bmatrix}^T$ in step 1, x and y load $\boldsymbol{F_{EE}} = \begin{bmatrix} -40\mathrm{N} & -40\mathrm{N} & 0\mathrm{N} \end{bmatrix}^T$ for step 2, and finally a load in x, y and z-direction $\boldsymbol{F_{EE}} = \begin{bmatrix} -40\mathrm{N} & -40\mathrm{N} & -40\mathrm{N} \end{bmatrix}^T$ for step 3. The results show a fair agreement at the end of the step responses but at the beginning there are overshoots, the maximum overshoot here is 5 N over a settling time of 30 sec. The settling time could not be reduced because this would have led to a greater overshoot. Thus the current platform is suited only for slow changes of prescribed forces at the end effector.

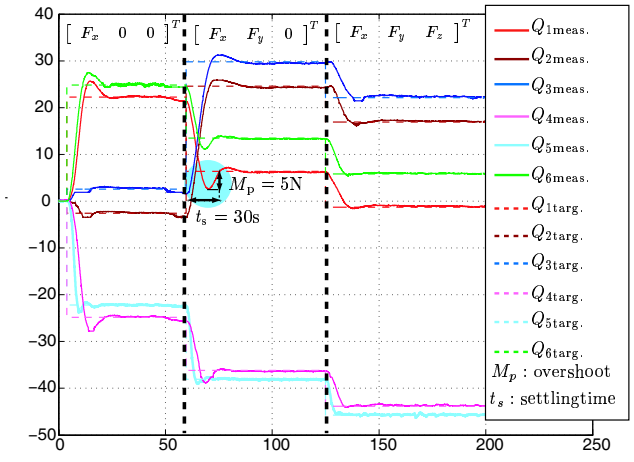

Figure 17: Resulting actuator forces Q_i for target wrench $\boldsymbol{w_{EE}}$

5 Conclusions

Presented in this paper is a novel six-legged parallel platform actuated by a combination of coaxial fluidic muscles and coiled springs. The platform is suited for force control, for which an appropriate control scheme is developed. The proposed force control uses an exponential approximation of the voltage step responses for inverting the gas model. As shown, this models is suitable for quasi-static force prescription. Future work will be devoted to designing an adaptive scheme which allows for faster transients and in particular helps to solve the problem of aging of the fluidic muscle parameters, which is significant.

Acknowledgment

The support of this project by the Deutsche Forschungsgemeinschaft under project numbers Ke 526/4-1 and Ke 526/4-2 is gratefully acknowledged.

References

[1] I. Davliakos and E. Papadopoulos. Model-based control of a 6-dof electrohydraulic Stewart-Gough platform. *Mechanism and Machine Theory*, 2008. in press.

[2] M. Dhanu-Singh, K. Liem, A. Kecskeméthy, and R. Neumann. Design and control of a pneumatic hybrid actuator. In *Proceedings of the 76th Annual Scientific Conference of GAMM*, pages 497 – 498, Luxembourg, Luxembourg, March 28 – April 1 2005.

[3] M. Dhanu-Singh, K. Liem, R. Neumann, and A. Kecskeméthy. Force control of a fluidic-muscle driven parallel platform. In *Proceedings of the 6th International Congress on Industrial and Applied Mathematics (ICIAM)*, Zurich, Switzerland, July 16–20 2007.

[4] Pernkopf F. and Husty M. L. Workspace classification of stewart-gough manipulators with planar base and platform. In *On Advances in Robot Kinematics*, pages 229–236, 2004.

[5] Merlet J.-P. Determination of 6d-workspace of gough-type of parallel manipulator and comparison between different geometries. Technical report, INRIA, Sophia-Antipolis, France, 1999.

[6] Merlet J.-P. *Parallel Robots*. Kluwer Academic Publishers, 2000.

[7] Merlet J.-P. A C++ algorithms library of interval analysis for equation systems, version 2.3. Technical report, INRIA, Sophia-Antipolis, France, September 2004.

[8] A. Kecskeméthy. M□BILE 1.3 *User's Guide*. Lehrstuhl für Mechanik, Universität Duisburg-Essen, 2003.

[9] Festo AG & Co. KG. *Fluidic Muscle MAS, Powerful, dynamic, stick-slip-free*. Festo AG & Co. KG., 2001.

[10] Marcel Langer. Flachheitsbasierte Regelung eines Fluidic-Muscles basierend auf experimentellen Kennfeldern. Diploma Thesis, Universität Duisburg-Essen, 2007.

[11] K. Liem, A. Kecskeméthy, and J.-P. Merlet. Hexaspine: A parallel platform for physical cervical spine simulation - design and interval-based verification. In *Proceedings of the 12th World Congress in Mechanism and Machine Science*, Besançon, France, June 17–21 2007.

[12] A. Lopes and F. Almeida. A force-impedance controlled industrial robot using an active robotic auxiliary device. *Robotics and Computer-Integrated Manufacturing*, 24:299–309, 2008.

[13] Carricato M. and Parenti-Castelli V. Singularity-free fully-isotropic translational parallel mechanisms. In *The Int. J. of Robotics Research*, pages 2(21):161–174, 2002.

[14] KUKA Roboter GmbH. *Robot Sensor Interface (RSI) Release 2.0*. KUKA Roboter GmbH, 2001.

[15] F. Ranjbaran, J. Angeles, and A. Kecskeméthy. On the kinematic conditioning of robotic manipulators. In *IEEE International Conference on Robotics and Automation*, volume 4, pages 3167–3172, Minneapolis, April 22-28 1996.

[16] Wey T. *Nichtlineare Regelungssysteme*. Teubner, 2002.

[17] Yoshikawa T. Manipulability of robotic mechanisms. *The Int. J. of Robotics Research*, 1(1), 1982.

[18] L.L. Whitcomb, S. Arimoto, T. Naniwa, and F. Ozaki. Adaptive Model-Based Hybrid Control of Geometrically Constrained Robot Arms. *IEEE Transactions on Robotics and Automation*, 13(1):105–116, 1997.

[19] X. Zhu, G. Tao, B. Yao, and J. Cao. Adaptive robust posture control of a parallel manipulator driven by pneumatic muscles. *Automatica*, 2008. in press.